HYDROLOGICAL PROCESSES
*Hydrol. Process.* (2011)
Published online in Wiley Online Library
(wileyonlinelibrary.com) DOI: 10.1002/hyp.8167

# Investigating the spatial distribution of water levels in the Mackenzie Delta using airborne LiDAR

C. Hopkinson,[1]* N. Crasto,[1,2] P. Marsh,[3] D. Forbes[4] and L. Lesack[5]

[1] *Applied Geomatics Research Group, Centre of Geographic Sciences, Lawrencetown, Nova Scotia*
[2] *Geology Department, Acadia University, Wolfville, Nova Scotia*
[3] *National Water Research Institute, Environment Canada, Saskatoon, Saskatchewan*
[4] *Geological Survey of Canada, Natural Resources Canada, Bedford, Nova Scotia*
[5] *Department of Geography, Simon Fraser University, Burnaby, British Columbia*

## Abstract:

Airborne light detection and ranging (LiDAR) data were used to map water level (WL) and hydraulic gradients ($\delta H/\delta x$) in the Mackenzie Delta. The LiDAR WL data were validated against eight independent hydrometric gauge measurements and demonstrated mean offsets from $-0{\cdot}22$ to $+0{\cdot}04$ m ($\sigma < 0{\cdot}11$). LiDAR-based WL gradients could be estimated with confidence over channel lengths exceeding 5–10 km where the WL change exceeded local noise levels in the LiDAR data. For the entire Delta, the LiDAR sample coverage indicated a rate of change in longitudinal gradient ($\delta^2 H/\delta x$) of $5{\cdot}5 \times 10^{-10}$ m m$^{-2}$; therefore offering a potential means to estimate average flood stage hydraulic gradient for areas of the Delta not sampled or monitored. In the Outer Delta, within-channel and terrain gradient measurements all returned a consistent estimate of $-1 \times 10^{-5}$ m m$^{-1}$, suggesting that this is a typical hydraulic gradient for the downstream end of the Delta. For short reaches (<10 km) of the Peel and Middle Channels in the middle of the Delta, significant and consistent hydraulic gradient estimates of $-5 \times 10^{-5}$ m m$^{-1}$ were observed. Evidence that hydraulic gradients can vary over short distances, however, was observed in the Peel Channel immediately upstream of Aklavik. A positive elevation anomaly (bulge) of >0·1 m was observed at a channel constriction entering a meander bend, suggesting a localized modification of the channel hydraulics. Furthermore, water levels in the anabranch channels of the Peel River were almost 1 m higher than in Middle Channel of the Mackenzie River. This suggests: (i) the channels are elevated and have shallower bank heights in this part of the delta, leading to increased cross-delta and along-channel hydraulic gradients; and/or (ii) a proportion of the Peel River flow is lost to Middle Channel due to drainage across the delta through anastamosing channels. This study has demonstrated that airborne LiDAR data contain valuable information describing Arctic river delta water surface and hydraulic attributes that would be challenging to acquire by other means. 

KEY WORDS channel; hydraulic gradient; DEM; laser intensity

*Received 5 October 2010; Accepted 12 May 2011*

## INTRODUCTION

### *Geographic context*

Arctic river deltas represent biological hotspots around the circumpolar Arctic that are both highly productive (Squires *et al*., 2009) and biodiverse (Galand *et al*., 2006; Lesack and Marsh, 2010) relative to the surrounding landscape. The high biodiversity is not well understood, but it may be due to the complex natural regime of water level fluctuations within these vast lake-rich systems that interconnect with complex networks of distributary channels (Lesack and Marsh, 2010). The Mackenzie Delta (Figure 1) in the Northwest Territories (NWT) is the second largest of the great Arctic deltas and contains around 45 000 lakes (Emmerton *et al*., 2007). Recent research has suggested its regime of both high-water and low-water levels may be changing as a consequence of reduced flow magnitude during river-ice breakup and a rise in relative sea level along the Beaufort Sea coast (Lesack and Marsh, 2007; Goulding *et al*., 2009). Given the size and low gradient of this system, relatively small changes in water level can affect large areas of habitat and substantially alter the natural variability that historically has existed. There is concern about the potential for landscape subsidence induced by extraction of natural gas from areas in the outer Mackenzie Delta because very low relief in this area could amplify the effect of even small changes in water levels (Lesack and Marsh, 2007; Forbes *et al*., 2010). Furgal and Prowse (2008) and Cohen (1997) have also outlined the importance of the water levels to navigation, socioeconomics, infrastructure stability, wild life and vegetation, and emergency preparedness within this region.

Recent International Polar Year (IPY) studies of the Mackenzie Delta have been conducted to improve the understanding of Arctic river delta water level regimes using hydraulic modelling (Nafziger *et al*., 2010) in combination with a broad suite of field experiments and other research activities (Marsh *et al*., 2010; Lesack *et al*., 2010). Water levels and channel hydraulic behaviour vary considerably with location and time of year, and are controlled by a number of factors, including discharge from the Mackenzie and Peel Rivers, storm surges, river

* Correspondence to: C. Hopkinson, Applied Geomatics Research Group, Centre of Geographic Sciences, Lawrencetown, Nova Scotia.
E-mail: chris.hopkinson@nscc.ca

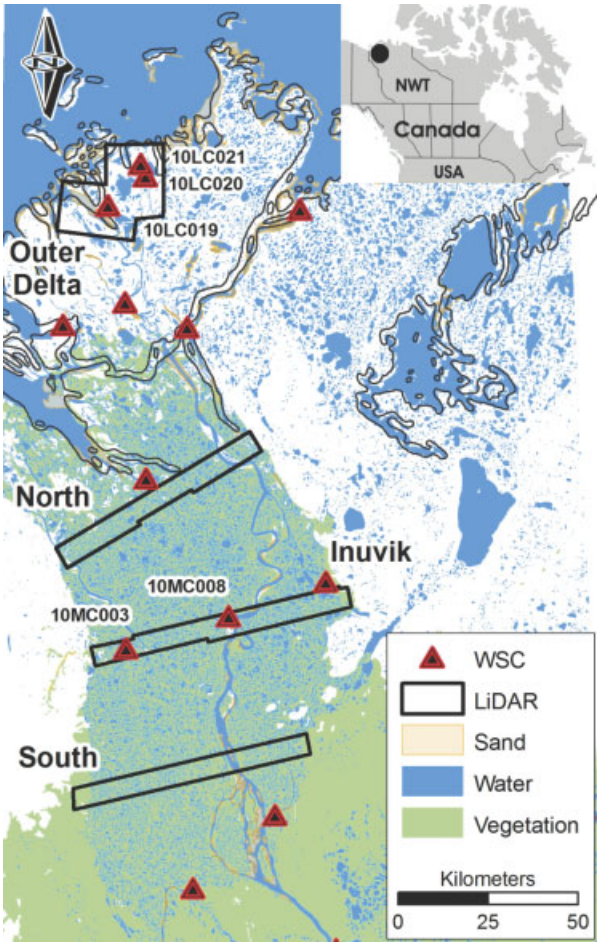


Figure 1. Study area including LiDAR coverage collected in 2008 and active WSC (Water Survey Canada) hydrometric stations (the five with station IDs are within areas surveyed by LiDAR and were used for water level validation)

ice, and tides (MRBC 1981; Marsh and Hey 1989; Hicks *et al*., 1995; Lesack and Marsh 2010). The manner in which this and other delta systems will respond to a warming climate and continued economic development requires data describing the spatial and temporal variability of the water level regimes in these systems. This is a daunting challenge given spatial water level variability within large floodplain environments can be difficult to characterize using traditional hydrometric station networks (e.g. Alsdorf *et al*., 2007a; Pavelsky and Smith, 2008).

While hydrometric networks are excellent at recording water level (WL) or height (H) variations through time ($\delta H/\delta t$) required to model changing discharge at a point, variations in discharge and WL with distance ($\delta H/\delta x$) within large and complex drainage basins are prone to significant uncertainty (Spence and Sasco, 2005). As channel slope reduces, so the proportional influence of an error in $\delta H/\delta x$ is amplified. Consequently, hydraulic calculations of discharge can be sensitive to boundary condition WL errors in areas of very low gradient, where channels can bifurcate and recombine to create anabranches or divide and spread out to form anastamosed networks of delta distributaries (Ivanov, 1970).

*Remote mapping of water levels*

This paper documents an experiment to evaluate the accuracy and efficacy of airborne light detection and ranging (LiDAR) for mapping channel water levels and gradients within the Mackenzie Delta. Given the large area and low gradients across the Delta, and logistical challenges with remote ground surveys and hydrometric equipment installations, airborne LiDAR (Wehr and Lohr, 1999) offers the potential to quickly and accurately generate terrain and water surface data to support regional hydraulic gradient research and model parameterisation. Such hydraulic applications have been demonstrated previously in remote and alpine landscapes (Hollaus *et al*., 2005; Mandlburger and Briese, 2007) and for temperate low-lying areas (Marks and Bates, 2000; French, 2003). Furthermore, derivations of inundation extent and high water lines around shorelines from LiDAR DEMs are becoming more common applications of LiDAR data in areas at risk of flooding (Lane *et al*., 2000; Genc *et al*., 2005). However, the use of topographic LiDAR systems to map water surfaces has received less attention.

Methods of direct classification of water extent using the geometric and intensity properties of LiDAR data have been demonstrated by Brzank and Heipke (2006) and Hofle *et al*. (2009). While direct water height or wave surface mapping is an implicit component of LiDAR bathymetry (Guenther *et al*., 2000; Hwang *et al*., 2000), few studies have evaluated the viability of airborne topographic LiDAR systems for spatial WL mapping (Shrestha *et al*., 1999; Carter *et al*., 2001; Magirl *et al*., 2005). An observation common to airborne and satellite LiDAR water sampling is high signal intensity or saturation when laser pulses encounter a specular water surface at a normal (or nadir) scan angle. Such signal saturation has the potential to introduce error into the estimation of water surface elevation (Urban *et al*., 2008) and will, therefore, be investigated.

One benefit of airborne LiDAR relative to *in situ* hydrometric or satellite-based WL estimates (e.g. Smith, 1997; Birkett *et al*., 2002; Alsdorf *et al*., 2007b) is that its spatial resolution and coverage are intermediate between these two observation methods and it thus offers a potential means to scale between them or to provide high-resolution validation for future satellite missions (e.g. SWOT: Surface Water Ocean Topography Mission—Durand *et al*., 2010). The Mackenzie Delta has 13 active hydrometric stations to represent thousands of kilometres of complex bifurcated anabranch and anastamosing channels. The temporal fidelity of these hydrometric records is good with continuous hourly data collected throughout the ice-free season available for most stations. Satellite WL observations can be made using RADAR (e.g. TOPEX/Poseidon, Jason-1, Jason-2) or LiDAR (ICESat) sensors, and these have been shown to offer temporal sampling with WL accuracies ranging from a few cms up to >1 m (Morris and Gil, 1994; Birkett, 2000; Martin *et al*., 2005; Urban *et al*., 2008). However, these are typically profiling sensors with large

footprint sample coverage (Alsdorf *et al*., 2007b) and are, therefore, limited to large water bodies exceeding several hundreds of metres across (Baghdadi *et al*., 2011). Hydrometric and satellite techniques can conceivably be combined but within a low gradient delta environment with thousands of lakes and variable size channels, uncertainties in along-channel hydraulic gradient or cross-delta stage variation will be inevitable.

Water surface gradients and stage variations in channels and lakes are critical to understanding the hydraulic behaviour of large deltaic and wetland systems, so in the absence of hydrometric gauge data, traditional field survey methods must be applied. Field crews can be deployed to survey WLs along channels or across the Delta but the resources required make the exercise impractical and costly. Even using helicopters, it is virtually impossible to manually sample water levels over an area the size of the Mackenzie Delta within sufficiently short time periods to be confident that the measurements are a static representation of the system. Assuming a nominal flying speed of 140 knots, an aerial survey of water levels across the full width of the Mackenzie Delta or along individual major channels lengths could be conducted in approximately 15 or 45 min, respectively. The speed with which airborne LiDAR can sample surface elevations, therefore, offers a potential advantage over manual WL survey techniques if it can be shown that the accuracy is sufficient to observe the hydraulic behaviour of interest.

The primary objective of this study is to quantify the precision, accuracy and any systematic bias in water level estimates derived from airborne LiDAR data within the low gradient environment of the Mackenzie Delta. A secondary goal is to present and discuss LiDAR-based observations of channel water level gradients within the Mackenzie Delta and place these observations within the physical hydrological context of the Delta environment. Given the size of the Delta and range of hydrological processes influencing water levels, this second objective is intended to be illustrative and to provide a platform for more focussed future research.

## METHODS

### *LiDAR data collection and processing*

As part of a broader IPY study of the Mackenzie Delta hydrology, airborne LiDAR data were collected between the 11 and 16 August 2008 during a period of late summer recessional flow, when WLs were about 1 m above annual baseflow levels (Figure 2). The data collection was planned and executed to meet several

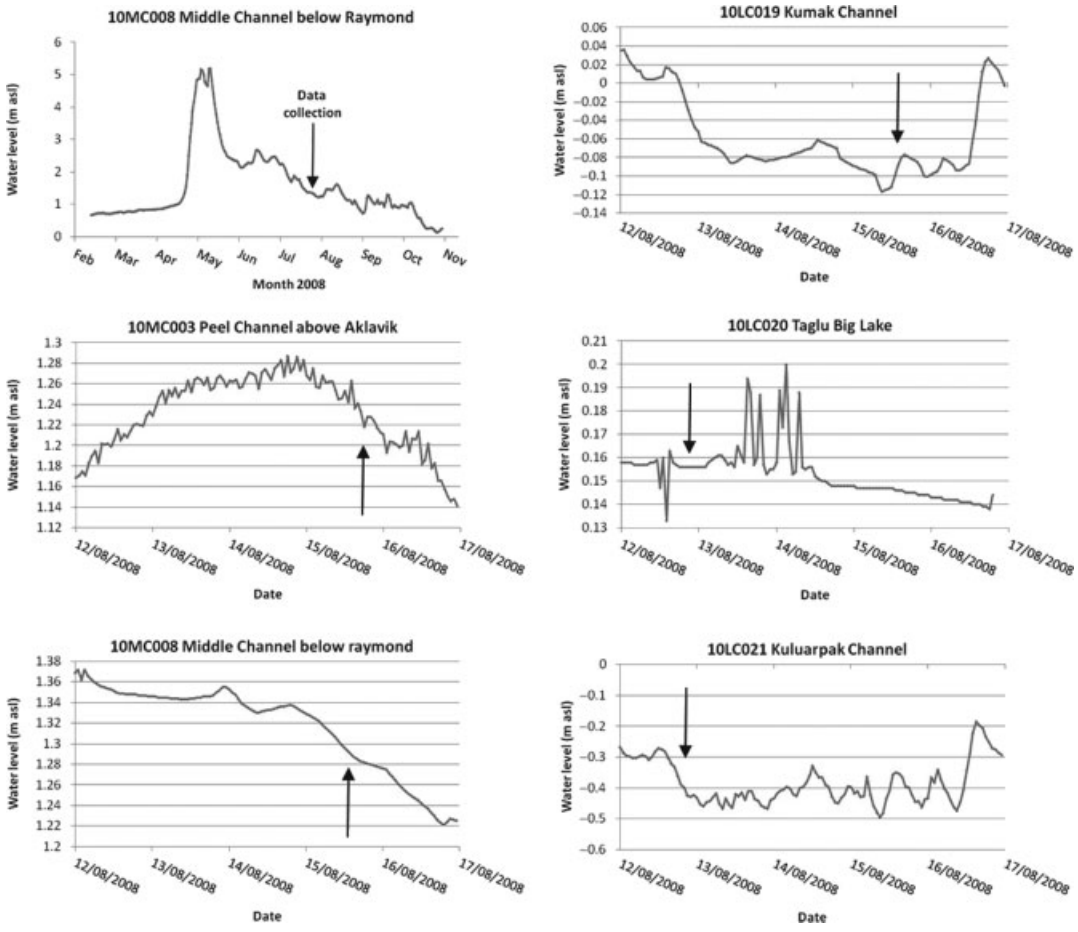


Figure 2. Water level hydrographs for hydrometric stations located within the LiDAR survey polygons. Black arrows indicate timing of LiDAR data collection over each station. Graph at top left, provides the annual WL context near the centre of the Delta. WSC station locations illustrated on Figure 1

 

research objectives, each with slightly different data and coverage requirements. Of these, the present study required that water levels could be validated against available hydrometric data and that spatial variation across the Delta and along channels could be investigated. To meet these experimental criteria, there was no need to survey the entire Delta, merely to sample water levels at strategic locations. The four polygons illustrated in Figure 1 met these (and other research question) criteria, while recognising that it would be too costly to fly the whole Delta with the research budget available. Indeed, not all the data collected were needed for or used in this study; rather, sample flight lines were extracted where necessary.

Three polygons ~70 km long × ~6 km wide covered the full width of upstream sections of the Delta; from upstream to downstream, these were referred to as the South, Inuvik, and North Transects (Figure 1). LiDAR data for a fourth, reverse 'L'-shaped survey area almost 30 km × 30 km (or 760 km$^2$) were acquired in the central section of the Outer Delta. The eastern polygon of this Outer Delta area (Taglu) was flown with a north–south orientation, while the west polygon (Niglintgak) was flown east–west. The flight time over each survey polygon ranged from 4 to 10 h. In all cases, an Airborne Laser Terrain Mapper (ALTM) 3100C (Optech, 2004) was used operating at a pulse repetition frequency (PRF) of 50 kHz and scanner field of view of 50°. All scan lines were flown with a 50% side lap to ensure the ground surface was surveyed from two different viewing geometries and the flying altitude varied between 1000 and 2000 m a.g.l. (above ground level) due to variable cloud conditions. The ground-level swath width varied from 950 to 1850 m. This range of data acquisition parameters ensured a ground-level sampling density of >0·6–1·4 pts/m$^2$. Point coordinates were projected in UTM zone 8 relative to the NAD83 CSRS reference frame, and elevations were given relative to the CGVD28 orthometric datum (see Appendix 1 for data processing and elevation transformation details). All laser pulse intensity data were range corrected to mitigate the systematic reduction associated with increased slant range bias at wide scan angles (Hopkinson, 2007):

$$I_{cor} = I_{obs} \frac{{R_{obs}}^2}{{R_{ref}}^2} \quad (1)$$

where $I$ = intensity, $R$ = range; and the subscripts *cor* = corrected, *obs* = observed, and *ref* = reference range, which in this case was the altitude of the aircraft above the ground surface.

Subsequent analysis of the LiDAR point cloud was conducted in two ways. For localized water level validation analyses the raw laser-point data were interrogated directly. For channel surface gradients along and across the Delta, laser-point data were converted to raster digital elevation model (DEM) grids, as this was computationally more efficient than handling over a billion irregular data points covering almost 2000 km$^2$. For each of the polygons, laser pulse returns collected within a single flight (thus, close in time) were converted to a 5 m raster DEM using an inverse distance weighted (IDW) algorithm (Shepard, 1968) with power function of two and search radius of 20 m. The IDW method was favoured over a straightforward triangulation interpolation because it can: (i) smooth out local noise in the data that might be captured using triangulation (McCullagh, 1981); and (ii) will not interpolate a surface outside of the 20 m search radius chosen. It was important not to generate surfaces in areas of large data voids, as surfaces in these areas would not be representative of the LiDAR data.

### *Water level validation*

Given the primary objective to quantify the precision, accuracy, and any sources of bias in airborne LiDAR water level data, the water level validation exercise was stratified into a number of specific tests. These three elements of uncertainty (precision, accuracy, and bias) were tackled first by evaluating the overall consistency or repeatability (precision) in data from flight line to flight line. Then absolute accuracy was evaluated by directly comparing LiDAR water levels to Water Survey of Canada (WSC) hydrometric station water level data that were coincident with the LiDAR survey areas. Finally, any systematic effects (bias) due to nadir (directly beneath the aircraft and normal to the water surface) high-intensity values were isolated by stratifying the LiDAR water elevation data into 'typical' and abnormally 'high' intensity classes.

For the first of these tests, regions of coincident LiDAR data within areas of large river channels, collected from temporally close (within 30 min) and spatially overlapping flight lines were identified and extracted within a 50 m diameter mask. To ensure the test was controlled and contained no potential bias due to high-intensity returns at nadir scan angles, comparative data were extracted from intermediate angles of the swath approximately midway between flight lines. Corresponding flight line pairs meeting these criteria were analysed for 12 spatially independent areas (>2000 LiDAR records) within the Inuvik transect and Outer Delta polygons.

Absolute water level validation was performed by first identifying the locations of WSC hydrometric stations that were both coincident with the LiDAR data and operating at the time of the surveys (Figure 1). When the locations were identified, LiDAR point data were extracted from a 50 m diameter mask adjacent to each hydrometric station and at least 30 m away from the bank to mitigate any influence of bank side waves and floating or emergent debris. All hydrometric gauges in the Delta have been recently referenced to the Inuvik GPS active control station and so are absolutely registered to the same reference point as the airborne LiDAR (see Appendix 2 for details on orthometric datum transformations). As with the LiDAR data, however, the hydrometric WL data also contain uncertainty due to: (i) the precision of the pressure transducer and data logging configuration used

 

($E_{PT}$); and (ii) uncertainty in the GPS positioning of the local station datum ($E_{GPS}$). Assuming the errors are normally distributed, the combined uncertainty ($E_{tot}$) from these two sources can be approximated by adding each component in quadrature:

$$E_{tot} = \sqrt{E_{PT}{}^2 + E_{GPS}{}^2} \quad (2)$$

The final test for systematic bias associated with nadir high-intensity values was similar to the first in that coincident point cloud data from the same flight line were extracted from within a 50 m diameter mask; high-intensity values were then identified and isolated. The intensity values are arbitrary numbers ranging from 0 to several thousand. For the purpose of this test, 'typical' intensity values were defined as all values (from all surface types) below the 95th percentile of the intensity distribution, and the outlying 'high' intensity values were defined as those within the upper 5th percentile. This class separation ensured that all points in the 'high' class were due to specular reflection from the water surface at nadir.

*Water gradients within the Delta*

Spatial water level variability within the Delta was investigated in two ways, each involving the generation of along-channel water surface profiles at 10 m sample intervals from the LiDAR DEM. Only channels that met the following criteria were examined: (i) had continuous LiDAR coverage (no obvious data voids) from the upstream to downstream edge of the transect; (ii) exceeded 60 m in width so that the influence of any interpolation-related bias at the bank side would be minimized (Note: examining raw point data directly would enable analysis for channel widths $< 5$ m); (iii) constitutes a single and distinct channel (i.e. not connected to an adjacent channel immediately up- or downstream of the transect). The first test was to examine along-channel slope and quantify whether or not the LiDAR WL sampling approach was appropriate for estimating hydraulic gradient in Delta environments. The linear best fit slope for each profile was recorded and tested to see if it was significantly different from a zero or null gradient at the 95% level of confidence. The second test was to summarize the mean WLs for each channel sampled and then plot the lateral distribution of major channel WLs across the Delta for the three upstream transect survey polygons. To place the WL distributions into the local terrain context, surface profiles along the east-to-west centre line of each polygon (and north-to-south in the Outer Delta) were also extracted.

## LIDAR WATER LEVEL OBSERVATIONS

*Water surface elevation precision between flight lines*

LiDAR water surface elevation data collected from coincident regions of overlapping flight lines demonstrated a mean absolute deviation of 0·04 m with individual flight line mean absolute differences ranging from 0·00 m to 0·11 m (Table I). Of the 12 flight line pairs compared, nine of the mean absolute differences observed were significant at the 95% level of confidence. These results are similar in magnitude to those observed over the runway control surface (Appendix 2), and therefore suggest that while significant differences between flight lines do exist, the overall LiDAR elevation precision is as good over water as it is over land. However, this is simply a test of consistency or repeatability for different flight lines and is not a measure of absolute accuracy. Furthermore, these results illustrate LiDAR water surface mapping behaviour at intermediate scan angles where nadir returns have no influence.

*Absolute water level validation*

A detailed description of the error components (Equation (2)) in hydrometric station water levels within the Mackenzie Delta is provided in Crasto (2011). In summary, $E_{PT}$ is assumed ~0·2% of the measurement

Table I. Summary of LiDAR water surface elevation comparison from overlapping flightlines (FL) at intermediate scan angles ($5° < \alpha < 20°$) collected over Inuvik and Outer Delta Polygons. All differences greater than 0·01 m are statistically significant at 95% level of confidence

| Polygon | FL-A | Avg H (m) | $\sigma$ (m) | $n$ | FL-B | Avg H (m) | $\sigma$ (m) | $n$ | Abs $\delta$H (m) |
|---|---|---|---|---|---|---|---|---|---|
| Inuvik (15 Aug) | 05 | −1·76 | 0·04 | 132 | 06 | −1·75 | 0·04 | 91 | 0·01 |
| | 06 | −1·80 | 0·03 | 100 | 07 | −1·76 | 0·05 | 99 | 0·04 |
| | 04 | −2·42 | 0·06 | 54 | 05 | −2·43 | 0·06 | 73 | 0·02 |
| | 03 | −2·56 | 0·05 | 97 | 04 | −2·47 | 0·04 | 29 | 0·11 |
| Outer Delta (15 Aug) | 34 | −0·23 | 0·07 | 65 | 35 | −0·17 | 0·08 | 56 | 0·06 |
| | 27 | −0·13 | 0·04 | 88 | 43 | −0·16 | 0·06 | 97 | 0·03 |
| | 38 | 0·23 | 0·01 | 90 | 45 | 0·23 | 0·01 | 146 | 0·00 |
| | 38 | −0·51 | 0·02 | 108 | 44 | −0·50 | 0·03 | 113 | 0·01 |
| Outer Delta (12 Aug) | 14 | 0·21 | 0·06 | 142 | 13 | 0·13 | 0·05 | 126 | 0·08 |
| | 11 | −0·49 | 0·06 | 131 | 10 | −0·52 | 0·07 | 119 | 0·03 |
| | 11 | −0·49 | 0·05 | 139 | 12 | −0·46 | 0·05 | 122 | 0·03 |
| | 09 | −0·02 | 0·08 | 113 | 10 | 0·03 | 0·08 | 98 | 0·05 |
| | | | | | | | **Mean$\delta$H** | | **0·04** |

Table II. Water level validation using active WSC hydrometric gauges located in areas coincident with LiDAR data coverage

| WSC Station | Polygon | Date and time (MST) | FL# | $H_{mean}$ CGVD28 (m) | $H_{mean}$ CGG05 (m) | $\sigma$ (m) | $n$ | WSC WL CGG05 (m) | $E_{tot}$ (m) | dH ($H_{lidar} - H_{WSC}$) (m) |
|---|---|---|---|---|---|---|---|---|---|---|
| 10MC008 | IVK | 11 Aug 20:00 | 1 | 1·45 | 1·41 | 0·11 | 51 | 1·37 | 0·05 | **0·04** |
| 10LC020 | OD | 12 Aug 21:00 | 6 | 0·10 | 0·06 | 0·07 | 1102 | 0·16 | 0·05 | **−0·10** |
| 10LC021 | OD | 12 Aug 21:00 | 9 | −0·38 | −0·42 | 0·04 | 912 | −0·43 | 0·05 | **0·01** |
| 10MC008 | IVK | 15 Aug 20:00 | 8 | 1·31 | 1·27 | 0·11 | 139 | 1·28 | 0·05 | **−0·01** |
| 10MC003 | IVK | 15 Aug 18:00 | 4 | 1·10 | 1·09 | 0·05 | 2232 | 1·22 | 0·05 | **−0·13** |
| 10MC003 | IVK | 15 Aug 19:00 | 5 | 1·01 | 1·01 | 0·04 | 2807 | 1·23 | 0·05 | **−0·22** |
| 10LC019 | OD | 15 Aug 11:00 | 27 | −0·16 | −0·12 | 0·01 | 464 | −0·11 | 0·05 | **−0·01** |
| 10LC019 | OD | 15 Aug 13:00 | 43 | −0·16 | −0·12 | 0·01 | 434 | −0·10 | 0·05 | **−0·02** |

scale (World Meteorological Organisation, 2010), which if applied to a WL measurement range of 20 m is ∼0·04 m. Typical long base line GPS errors ($E_{GPS}$) using modern equipment are ∼0·02 m. Therefore, the estimated combined uncertainty ($E_{tot}$) for water level data is ∼0·05 m. Hydrometric water levels are averaged over a 1-h period, while LiDAR estimates are instantaneous and therefore susceptible to short-lived WL aberrations near the gauge site. For this reason, 0·05 m is considered an optimistic estimate of uncertainty associated with the true WL to which LiDAR observations are compared.

For the five WSC hydrometric stations inside the LiDAR polygons, it was possible to make eight independent sets of WL comparisons (Table II). The overall mean offset was −0·06 m (max = 0·04 m, min = −0·22 m), with 3 of the 8 observed offsets being significant at the 95% level of confidence. These observations are comparable to the runway validation which demonstrated a mean bias of −0·01 m to −0·11 m, with a total mean bias of −0·05 m (Appendix 2). Furthermore, the mean offset is close to the estimated uncertainty in the hydrometric gauge WL observations of 0·05 m. Therefore, these results suggest that the error in water surface elevation is, on average, no worse than it is over land surfaces. However, the greatest negative bias (−0·22 m) was observed at the Peel Channel hydrometric station (10MC003), which was almost directly beneath the centre line of the associated LiDAR flight track, i.e. the associated LiDAR data were collected near nadir and displayed higher laser signal intensities than at other gauge sites.

*Influence of near-nadir high-intensity returns*

*Laser intensity range bias.* As expected with laser-based ranging over water surfaces (Urban *et al*., 2008), a systematic clustering of saturated and high-intensity returns near nadir of the flight track is clearly visible in the image of laser pulse return intensity over a section of the North Transect (Figure 3). In this example, the flight lines are spaced a little over 1000 m apart and the zone of high intensity due to specular reflectance off the water surface is visible up to 200 m either side of the flight line. For the survey altitude of 2000 m a.g.l., this corresponds to <5° off nadir. The adjacent land surfaces demonstrate no systematic intensity variation because they have more Lambertion properties.

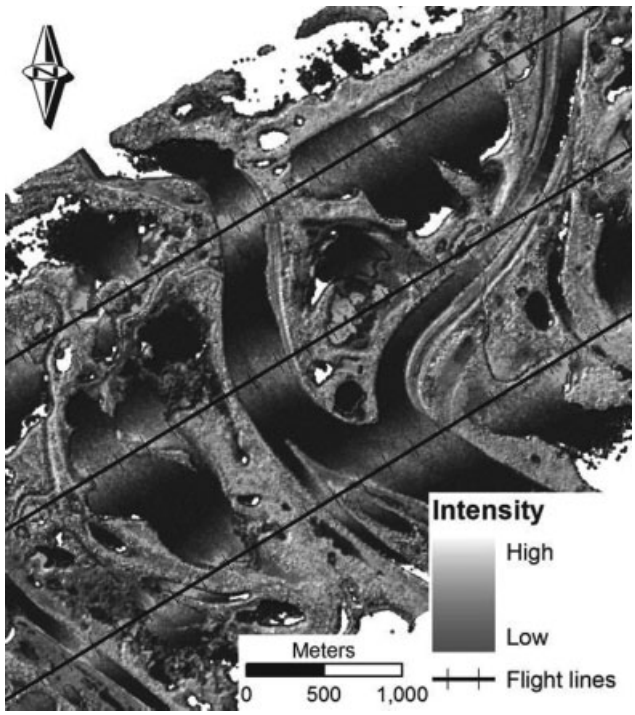


Figure 3. LiDAR intensity image captured in vicinity of Napoiak Channel in the centre of the North Transect. Note how intensity increases at nadir and data density decreases away from nadir due to specular reflection from the water surface

After interrogating the intensity distribution of the LiDAR datasets, it was found that the 95th percentile value lay in the range of 140–150. Consequently, '150' was adopted as the intensity threshold value for high-intensity returns. The relative difference in water level when LiDAR returns displaying high intensities were compared to those displaying more typical values is illustrated in Table III. For four flight lines in the Inuvik Transect there is a small systematic negative bias of approximately −0·05 m in elevation associated with high intensity values. Three of the five flight line samples in the Outer Delta also demonstrate a negative bias, with two of these being significant at the 95% level of confidence.

The laser ranging mechanism utilized by the ALTM 3100 is a time interval meter (TIM) that records the travel time between pulse emission from the laser transmitter to reflected pulse return at the receiver (Wehr and Lohr,

Table III. LiDAR-based water level bias associated with nadir high-intensity returns for nine in-channel sample areas in the Inuvik Transect (IT) and the Outer Delta (OD) collected on 15 August

| Flight line | Water level (m a.s.l. [CGVD28]) | | | |
|---|---|---|---|---|
| | I >150 | I <150 | $\delta$Z | *p*-value |
| IT (1) | −1·88 | −1·83 | −0·05 | >0·05 |
| IT (2) | −1·85 | −1·82 | −0·03 | >0·05 |
| IT (3) | −2·16 | −2·12 | −0·04 | >0·05 |
| IT (4) | −2·14 | −2·08 | −0·06 | >0·05 |
| OD (1) | −6·32 | −6·32 | 0·00 | **0·68** |
| OD (2) | −6·32 | −6·31 | −0·01 | **0·19** |
| OD (3) | −6·06 | −6·04 | −0·02 | >0·05 |
| OD (4) | −6·18 | −6·16 | −0·02 | >0·05 |
| OD (5) | −6·18 | −6·18 | 0·00 | **0·57** |

1999; Petrie and Toth, 2009). There are various mechanisms available for triggering the TIM but one of the most robust methods, and the one used within the ALTM, is a constant fraction discriminator (CFD) (Wagner *et al*., 2004). However, no laser pulse triggering mechanism will provide perfectly consistent time thresholding under the range of signal intensities experienced by a commercial airborne laser ranging device. The signal-to-noise characteristics of a laser pulse passing through a CFD are such that abnormally high-intensity pulses will be tagged slightly early, while low-intensity pulses may be tagged slightly late. This early or delayed trigger of the TIM systematically results in high-intensity returns displaying short ranges with low-intensity returns displaying long ranges. To compensate for these systematic CFD and TIM biases for outlying intensity values, and improve overall system accuracy over typically encountered surfaces, a factory calibration is conducted on all ALTM devices that adjusts the range based on the laser pulse intensity recorded (Figure 4).

Given that high-intensity pulses tend to trigger the TIM early, resulting in a positive elevation bias, the calibration curve illustrated in Figure 4 increases ranges by up to 0·25 m for high-intensity returns. Conversely, range is reduced by up to 0·1 m for weak or low-intensity returns.

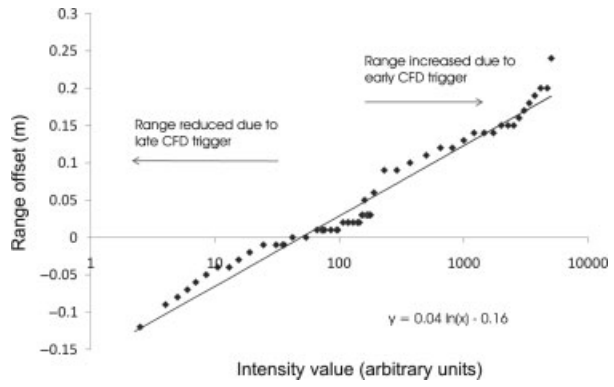


Figure 4. Intensity-based factory calibration corrections applied to ALTM 3100 range measurements. The calibration varies with sensor pulse repetition frequency. Illustrated here is the calibration curve for the 50 kHz configuration adopted for the Mackenzie Delta surveys

The observation that high-intensity data corresponds to a negative WL elevation bias (Table III) indicates, therefore, that the factory calibration curve has actually over compensated for the systematic bias in the CFD trigger mechanism. This is presumably because the intent of the intensity-based range calibration is to increase accuracy over typical Lambertion terrestrial targets as opposed to specular water surfaces. This bias could be mitigated in one of two ways: (i) All LiDAR records displaying high-intensity values can be removed. In areas where specular reflection is minimal, this should not pose a problem, as the proportion of high intensity returns will be small. However, at nadir scan angles where the surface behaves like a specular reflector, removing the data will create voids and is potentially counter-productive. (ii) If water areas can *a priori* be masked or classified (e.g. Brzank and Heipke, 2006; Hofle *et al*., 2009), then it would be possible to apply *a posteriori* a positive correction that would compensate for the bias. However, even though the bias observed is systematic it is still smaller than the accuracies quoted by the manufacturer (Optech, 2004) and within the range of observed error at the terrestrial control and validation sites (Appendix 2).

*Water surface properties and laser intensity.* The observation that channel surface elevations in the Inuvik Transect and Outer Delta areas display different levels of intensity-related bias (Table II) requires investigation. Examining the mean intensity for those data in the high class indicates that, overall, the Inuvik Transect has a higher proportion of intensities above 150 than the Outer Delta, with the mean value in this class being almost 100 above that for the Outer Delta. From Equation (1), it can be predicted that over the same surface, intensity values in the Inuvik Transect will be approximately 23% higher than in the Outer Delta due to a 200 m difference in flying altitude. This reduced mean intensity over the Outer Delta can account for <0·02 m (or ∼50%) of the difference (Figure 4) but not all of it. Therefore, there appears to be something physically different between the Outer Delta and Inuvik Transect channel water surfaces that has altered the intensity response and subsequent elevation bias associated with nadir returns.

The simplest explanation for a subdued intensity response at nadir is that the Outer Delta channels possessed slightly increased Lambertion properties relative to the highly specular response of the Inuvik Transect channels. Two possibilities are postulated: (i) sediment concentrations in the Outer Delta channels may have been elevated relative to those upstream due to local tide effects (e.g. Hill *et al*., 2001) and thus altered the optical properties of the water surface. However, this is not thought to be a dominant factor as even saturated estuarine mudflats display extremely high intensity values at nadir (e.g. Brennen and Webster, 2006); (ii) The channels in the Outer Delta are wider, have shallower levees and less vegetation cover than upstream (Mackay, 1963). Consequently, the Outer Delta channels that are adjacent to the ocean have far greater exposure to wind effects.

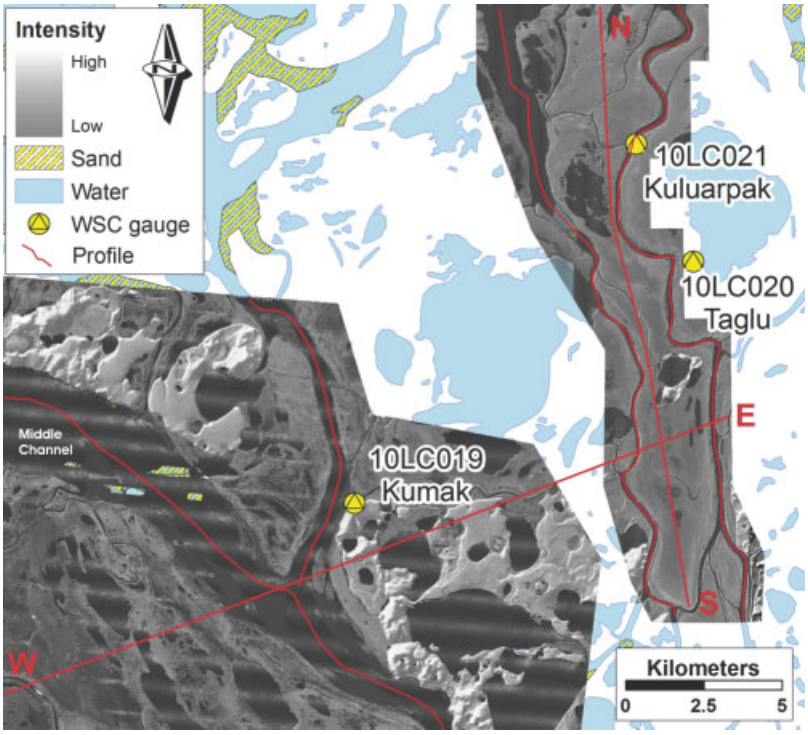


Figure 5. Partial lidar intensity image for the Taglu (left) and Niglingtak (right) polygons within the Outer Delta. Channel water surface and terrain profiles are highlighted, as are three of the WSC hydrometric stations used in the WL validation. Note the higher intensities visible at nadir in the Niglintgak polygon, which was collected on a different day

It is reasonable to postulate, therefore, that wind disturbance over the water has led to increased surface texture and thus reduced its specular reflectance properties. This is important to note, as it implies that a bias will not always be present for nadir returns but only in situations where the water surface has highly specular properties leading to a very high and/or saturated intensity response at nadir scan angles.

## MACKENZIE DELTA SURFACE AND WATER LEVEL GRADIENTS

### *Outer Delta area*

Surface gradients were evaluated along 10 m increment sampling profiles over both terrain and channels. The locations of these profiles in the Outer Delta polygons (Taglu and Niglintgak) are illustrated in Figure 5. The flight lines collected over the Taglu polygon were oriented north to south and incremented from east to west on 12 August. For the Niglintgak polygon, collected on 15 August, the flight lines were oriented east to west, starting four flight lines north of the Kumak Channel bifurcation from the Main Channel. The lines tracked to the southerly extent before returning to the start point and tracking north. From start to finish, each polygon took ~3·5 h to complete. For the Kumak and Middle Channels in the Niglintgak polygon, it took ~3 h to sample the full channel lengths, while for the channels in the Taglu polygon, each channel was completely sampled in less than 1 h.

The four Outer Delta channel LiDAR WL profiles are presented in Figure 6. Along all profiles, the range of 'noise' (local maxima and minima) reaches 0·2 m in places yet statistically significant slope gradients ($p$ <0·05) are observed for all best fit lines through the data. Considering only temporally contiguous flight line data, the gradients on all four channels are equivalent at $-1 \times 10^{-5}$ m m$^{-1}$ (or 1 cm per km). This despite the LiDAR overflights occurring three days apart during flow recession at Kuluarpak and steady flow at Kumak (Figure 2).

In Middle Channel, the influence of the Beaufort Sea is evident in the WL elevation drop of ~0·2 m at around the 19000 m point in the profile (Figure 6). This occurred, as there was a ~2·5 h break in the LiDAR sampling at this point. This suggests tides or other hydrodynamic phenomena can affect hydraulic gradient observations in the outer extremities of deltaic systems, and any WL sampling must be temporally continuous along the reach and conducted over as short a time span as possible. However, it is worth pointing out that the observed WL drop over this time period suggests that the Middle Channel WL was receding at ~0·08m hr$^{-1}$. This in itself could be valuable information if attempting to model the hydrodynamics of this system; especially as a similar drop was not observed within the adjacent Kumak Channel (Figures 2 and 6).

No field or gauge data describing channel gradient were available to support this study but it is worth noting that the best fit slope gradient observed in the north to south terrain profile adjacent to Kuluapak Channel (Figures 5 and 7) also demonstrates a trend of $-1 \times$

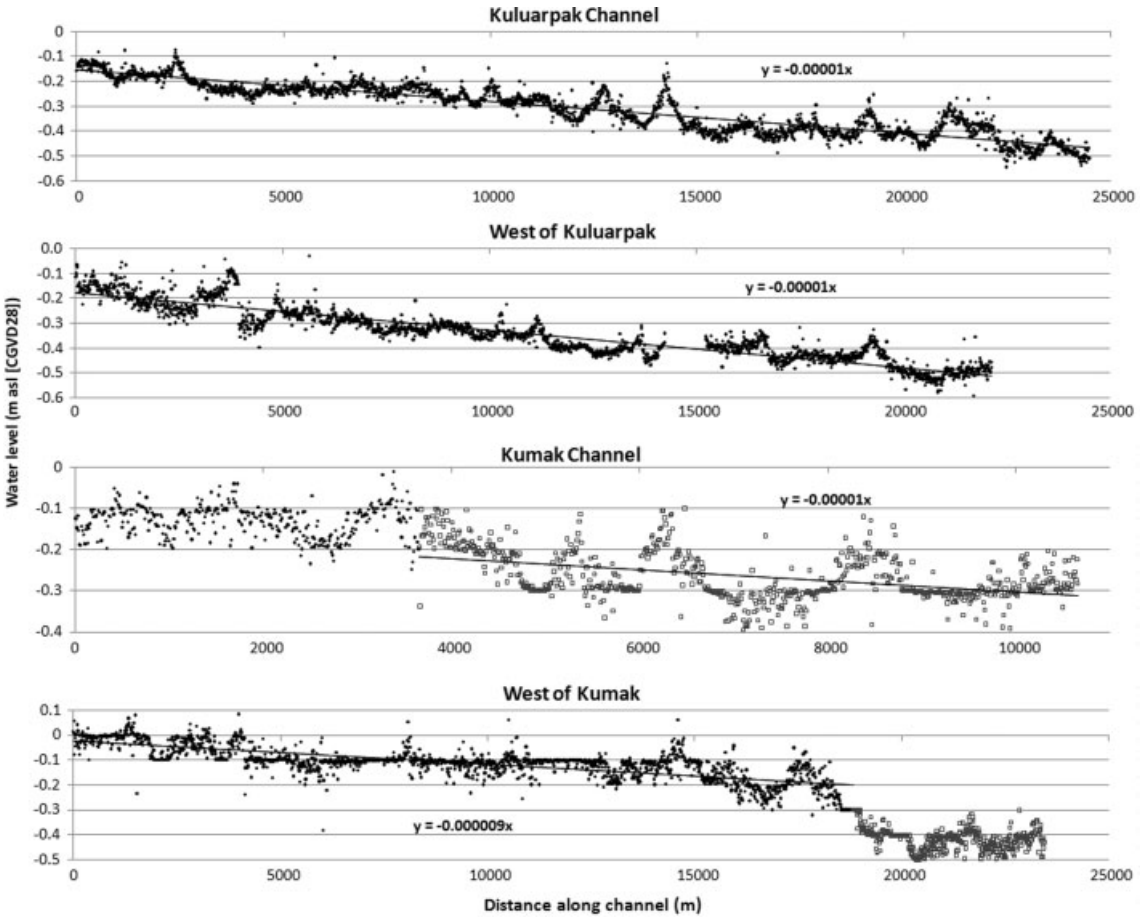


Figure 6. WL profiles and average slope gradients for channels extracted from the LiDAR DEM in Taglu and Niglintgak polygons. The average gradient line for the Kumak and Middle Channels is only provided for temporally contiguous flight lines. Black dots = initial contiguous channel sampling; grey squares = altered configuration for Kumak and Middle channels

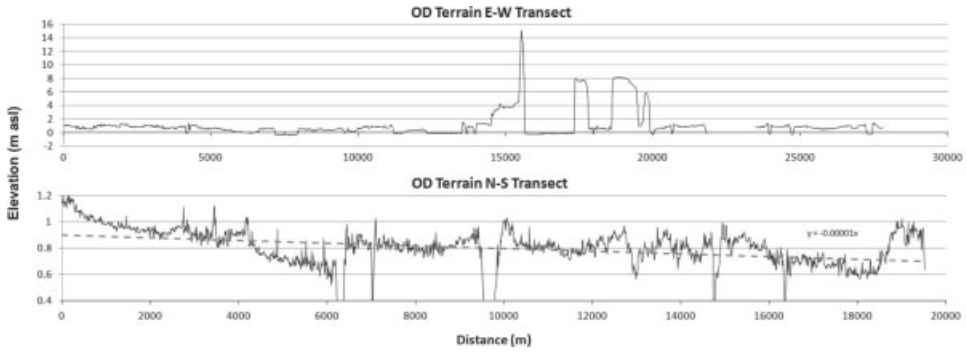


Figure 7. DEM surface profiles from west to east (top) and south to north (bottom) across the Outer Delta LiDAR polygons (profile locations illustrated in Figure 5)

$10^{-5}$ m $m^{-1}$ for the outer 20 km of the Delta before reaching the ocean. Given the same gradient is observed in the terrain and over four channels sampled during rising and receding flow conditions, this is likely a typical hydraulic gradient for large channels in the Outer Delta area during the recession period, and for periods when there are no large WL variations due to spring breakup, large summer rain events or storm surges.

*Inuvik Transect*

In the Outer Delta, obtaining statistically significant hydraulic gradients was straight forwards, as contiguous LiDAR coverage is up to 20 km and the observed gradient is such that the local noise level is exceeded for a channel reach of 10 km. However, the maximum contiguous LiDAR coverage in the approximate channel flow direction (south to north) for upstream survey polygons is 3·5 km for the Inuvik Transect. The North Transect was completed over three flights and has no complete contiguous coverage across the Delta, while the South Transect never exceeds 2·4 km in width. The observed noise level in LiDAR WL data is generally <0·1 m (Tables I and II) with periodic deviations exceeding this amount due to nadir high intensity influences (Table II

 

Table IV. Centre-line profile lengths and gradients extracted for channels exceeding 60 m width and displaying continuous LiDAR coverage across the Inuvik Transect

| | Peel River @ Aklavik | Channel # 2 | Middle Channel | East Channel @ Inuvik |
|---|---|---|---|---|
| Profile distance | 0 | 15 | 31 | 60 |
| Length (km) | 10 | 9 | 5 | 3·8 |
| Slope ($\delta$H/$\delta$x) | $-5 \times 10^{-5}$ | $+2 \times 10^{-6}$ | $-5 \times 10^{-5}$ | $-3 \times 10^{-6}$ |
| $\sigma$ (m) | 0·07 | 0·05 | 0·07 | 0·05 |
| $p$-value | <0·05 | 0·12 | <0·05 | 0·18 |

and Figure 6). Therefore, to accurately quantify a WL gradient, the length of channel reach sampled needs to be long enough that $\delta$H exceeds the noise that occurs over $\delta\times$. This was tested by examining the WL profiles extracted from four main channels crossing the full width of the Inuvik Transect (Table IV).

The channels in the centre of the Delta tend to meander such that even though the contiguous section of the Inuvik Transect was only 3·5 km wide, channel lengths of up to 10 km were profiled (Table IV). Of the four channels meeting the size and coverage criteria adopted, two displayed gradients that were significantly different from zero (Peel Channel and Middle Channel). Moreover, the gradients estimated were similar to other findings for this part of the Delta by Marsh and Hey (1989). One channel did display a positive gradient (i.e. apparently rising water level downstream) but this was not statistically significant ($p = 0{\cdot}12$). These observations suggest that for hydraulic gradients typical of the Mackenzie Delta and for WL noise levels of ~0·1 m, >5–10 km of contiguous airborne LiDAR data is needed along a channel reach in order to confidently estimate the gradient. However, this assertion is premised on the assumption that the statistically insignificant observation of a positive gradient, such as for 'channel # 2' (Table IV), is false. While a continuous positive gradient along 9 km of river channel is unlikely, a closer examination of the Peel Channel profile suggests that positive gradients over short sections can occur (Figure 8).

The Peel Channel undergoes a tight double meander near the Aklavik town site and hydrometric station (10MC003), and it has been noted as a region of occasional extreme bank erosion (Mackay, 1963). LiDAR-based water levels collected from 4 contiguous flight lines within a 1-h period illustrate a bulge of >0·1 m in the water surface between points 'B' and 'E' in Figure 8. This region corresponds to a reduction in channel width from 320 m at point 'B' to 120 m at point 'C', followed by a sharp meander from 'D' to 'E'. The WL profile does possess obvious areas of localized negative bias associated with nadir high-intensity laser pulse returns, but these local artefacts do not affect the general trend in the data. Errors in the flight line GPS trajectory cannot be completely ruled out but this is unlikely given the gradual rise and fall from flight line to flight line through 'B' to 'E', and given WLs do indeed drop as expected beyond 'E' despite being sampled by the same flight lines. This observation suggests that the constriction near the anabranch at point 'C' is holding up flow through this part of the channel. The channel and flow conditions necessary to cause such a localized increase in head is worthy of future study.

Table V. Mean elevation, gradient and rate of change in gradient estimated from centre line profiles of each survey polygon across the Delta

| | South | Inuvik | North | OD |
|---|---|---|---|---|
| Elevation (H) | 6·29 m | 3·61 m | 1·91 m | 1·12 m |
| Distance (x) | 0 km | 41 km | 82 km | 167 km |
| Slope ($\delta$H/$\delta$x) | $-6{\cdot}5 \times 10^{-5}$ | $-4{\cdot}1 \times 10^{-5}$ | $-9{\cdot}4 \times 10^{-6}$ | |
| $\delta^2$H/dx | $-5{\cdot}1 \times 10^{-10}$ | $-5{\cdot}8 \times 10^{-10}$ | | |

### *The entire Delta*

The mean longitudinal gradient for the entire Delta was reconstructed from the west-to-east DEM centre-line surface profiles (terrain and water) across the four polygons surveyed (Figures 7 and 9). While gradients can be calculated from point to point along the Delta using traditional survey methods, the high-resolution LiDAR DEM captures millions of ground and water surface elevations across the full width of the Delta. Consequently, an accurate mean elevation for the entire Delta cross-section is possible. By comparing the mean surface profile elevations at each W-E centreline and measuring the linear distance between the centre points of each profile, the DEM gradient was found to range from $-6{\cdot}5 \times 10^{-5}$ m m$^{-1}$ in the upstream part of the Delta to $-9{\cdot}4 \times 10^{-6}$ m m$^{-1}$ at the downstream end (Table V). The gradient between North Transect and Outer Delta being statistically equivalent to those observed in the channels and terrain of the Outer Delta polygons (Figures 6 and 7). The gradient observed between Inuvik and North Transects is within the range reported by Marsh and Hey (1989) for the East Channel in the same part of the Delta. Having four accurate elevation samples along the length of the delta enables three estimates of gradient and further allows for two estimates of the rate of change in gradient (Table IV). The rate of change in gradient observed in the upper and lower Delta is similar, suggesting that a single mean value of $-5{\cdot}5 \times 10^{-10}$ m m$^{-2}$ is a reasonable first approximation of the overall trend. Knowing the rate of change in gradient means that the average gradient for

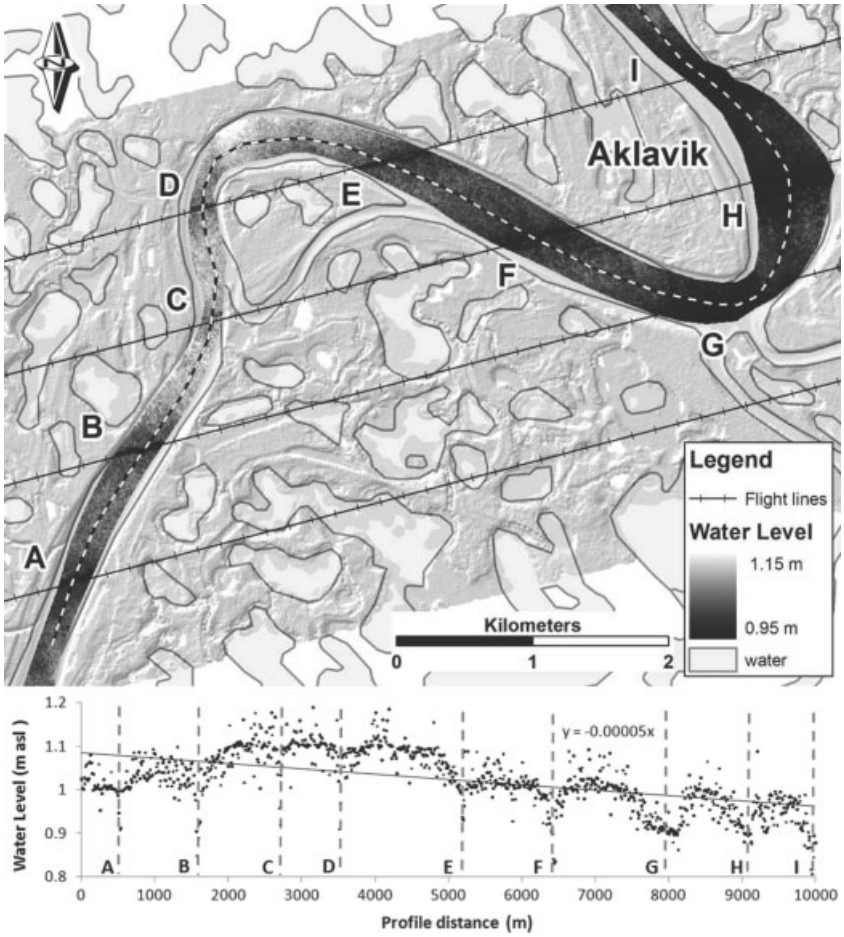


Figure 8. Shaded relief LiDAR DEM of Peel River at Aklavik with flight lines and water surface elevation image overlaid (top). Plot of water surface elevation along the profile (bottom). Letters A to I illustrate flight line and channel intersection points

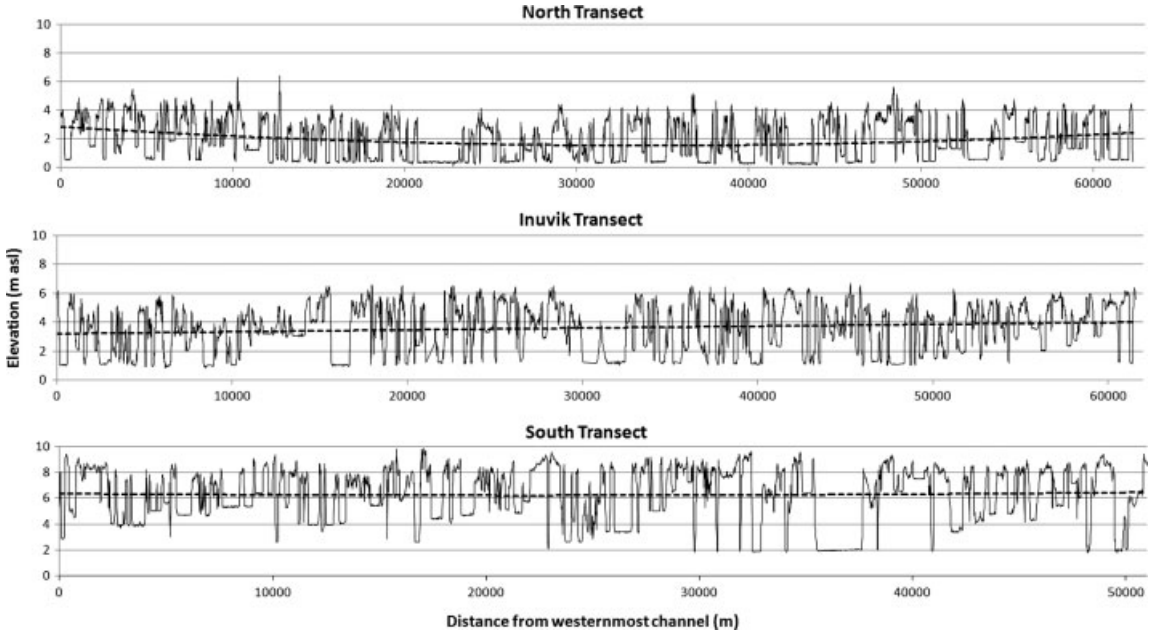


Figure 9. DEM surface profiles from west to east for the three upstream 'Transect' polygons covering the full width of the Delta. Each profile starts at the westernmost channel and ends at the easternmost channel within the Delta. A quadratic best fit line is plotted to illustrate the general trend in surface elevation

any section of the Delta can be estimated. This characterisation of the changing surface gradient along the Delta can potentially be used to assist hydraulic model setup.

Given the gradient estimates in Table IV are taken from DEM surface profiles that include both terrain and water surfaces, they do not necessarily represent

 

the late summer hydraulic gradients within channels. For example, the terrain surface is known to possess a higher gradient than late summer WLs (Mackay, 1963) due to local bank heights being greater upstream, with levee and water level elevations tending to converge downstream. However, these synoptic gradient estimates likely do approximate the general water surface condition throughout the Delta when WLs are at flood stage.

*Cross-Delta gradients*

Thus far, discussion has focussed on WL gradients in the general south to north direction of in channel flow. Given the size and complexity of the Mackenzie Delta channel network, there is considerable justification for characterising any lateral or 'cross-Delta' gradients in WLs. No consistent or systematic gradients are apparent across the LiDAR DEM surface profiles (Figure 9). However, examining the mean channel WLs during a 24-h period of summer low flow across these three transects does reveal some interesting patterns (Figure 10). The reduced number of intermediate and large channels (>60 m wide) within the Inuvik Transect (15 August) demonstrate no significant cross-Delta gradient and mean channel WLs are all within 0·2 m. Both the North and South Transect profiles (16 August) demonstrate significant deviation from a zero gradient, which in both cases can be described by a parabolic curve (Figure 10). For the North Transect, the curve is almost symmetrical around the Napoiak Channel, which is consistent with a process of drainage from the margins of the Delta toward the larger channels in the centre (and consistent with the DEM profile in Figure 9). The South Transect, however, demonstrates that in the upstream section of the Delta, there is a systematic lateral gradient from the Peel River channels on the west side to the Middle Channel of almost 1 m, despite no gradient being observed in the DEM (Figure 9).

Comparing the WSC hydrometric records for the Peel Channel at Aklavik (10MC003) and the Middle Channel of Mackenzie River below Raymond (10MC008) during August 2008, it is found that WLs are slightly

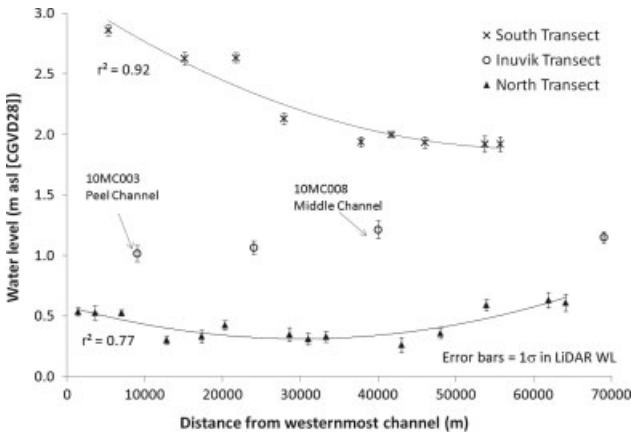


Figure 10. Mean water levels in main channels at each of the three Transect polygons across the Mackenzie Delta. Quadratic best fit lines applied to North and South Transects

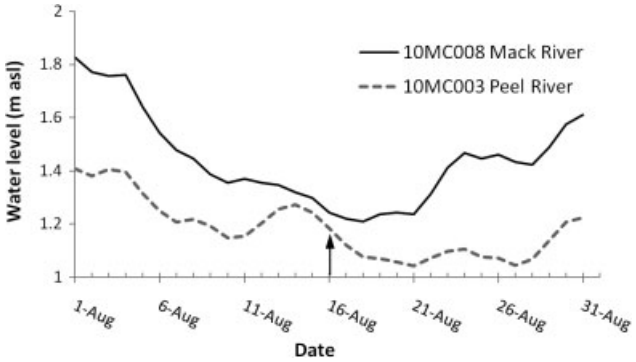


Figure 11. Water levels at Peel and Mackenzie Rivers along the Inuvik Transect for month of August. The arrow indicates the time of LiDAR acquisition for the South Transect WLs illustrated in Figure 10

lower on the west side (Peel Channel) than Middle Channel (Figure 11). This corroborates the LiDAR WL data across the Inuvik Transect but contrasts markedly with the upstream condition along the South Transect (Figure 10). The gauge records further indicate that at the time of the South Transect LiDAR acquisition, the Peel Channel at Aklavik was on the recessional limb of a distinct flow pulse that was largely absent on the Mackenzie. Unfortunately, the hydrometric station for Peel River at Frog Creek where the river enters the Delta (10MC022) was not active during this period, so the flow entering the Peel anabranch channels upstream of Aklavik is unknown.

On the basis of the flow pulse observed in the Peel on the west side of the Delta in the Inuvik Transect (Figure 11) it is likely that the high water levels on the west side of the south Transect (Figure 10) were partially associated with this flow pulse. However, given the flow pulse was receding, and water levels on the Peel were lower than Middle Channel within the Inuvik Transect, the observation of higher upstream water levels on the Peel the following day requires explanation. If increased flow caused the increased WLs in the LiDAR South Transect data, this is incongruent with recessional flow and reduced WLs downstream unless drainage through the SW region of the delta is being preferentially drawn over to the Middle Channel of Mackenzie rather than continuing along the Delta within the Peel channels. An analogous situation was documented by Emmerton *et al*. (2007) where discharge drops were observed along sections of the East Channel, and the only plausible explanation was that flow was being scavenged by the lower elevation Middle Channel. These observations, therefore, highlight the importance of cross-Delta hydrological fluxes and the need for accurate lateral WL gradient information.

## CONCLUSIONS

An objective of this study was to test whether or not airborne LiDAR was sufficiently accurate and consistent to measure channel water levels and hydraulic gradients in a large Arctic deltaic environment displaying small

changes in elevation over large distances. The results of the WL validation (Table II) indicate that for the LiDAR dataset collected over the Mackenzie Delta in 2008, uncorrected mean deviations lay in the range of −0·22 to +0·04 m, with standard deviations between 0·01 and 0·11 m. Some of the negative elevation bias was attributed to a systematic over-correction of high signal intensity LiDAR range measurements at near-nadir scan angles (Table III). In general, LiDAR-based WL gradients could be computed for channel lengths longer ∼5–10 km, and where the WL change exceeded the ∼0·1 m noise level of the LiDAR data. However, to reliably assess WL gradients it is important to minimize survey time by flying parallel to the predominant channel flow direction, or by flying lines contiguously over channels with tidal influences, or otherwise rapidly changing water levels

In the Outer Delta, 4 gradient measurements for channel reaches of 5–25 km long, plus one profile across the terrain surface, all returned a consistent estimate of $-1 \times 10^{-5}$ m m$^{-1}$. This value was further corroborated in the elevation change observed from the North Transect to the Outer Delta, suggesting that this is the typical hydraulic gradient for the downstream end of the Delta. Further upstream, longitudinal gradients between the cross-Delta DEMs lay between 4 and $7 \times 10^{-5}$ m m$^{-1}$ with an apparent rate of change in gradient ($\delta^2$H/$\delta$x) of $5{\cdot}5 \times 10^{-10}$ m m$^{-2}$ along most of the Delta. Within-channel gradients in transect polygons could not be reliably extracted over short channel lengths, but in two cases in the Inuvik Transect, significant and consistent estimates were extracted from the Peel and Mackenzie Rivers, indicating a value of $-5 \times 10^{-5}$ m m$^{-1}$. These measurements represent local conditions on channels less than 10 km in length and, therefore, do not necessarily represent the gradient over longer distances. Evidence that gradients vary over short distances was observed on the Peel Channel immediately upstream of Aklavik. An elevation anomaly (bulge) of >0·1 m was observed at a channel constriction entering a sharp meander bend. The 'bulge' in the water surface was evident across three independent flight lines and covered a stretch of channel exceeding 3 km.

Of some hydrological significance, it was also observed that late summer water levels in the anabranch channels of the Peel River draining through the southwest region of the Delta were almost 1 m higher than in Middle Channel. However, in the area where the Peel anabranch channels recombine to form a single channel at Aklavik, the water levels were similar to that of the Middle Channel. For the cross-Delta profiles in this area (Figure 9), the terrain elevations demonstrated no significant gradient. These observations were made at a time when the Peel River was in recessional flow following a recent event. Possible explanations include: (i) the channels are elevated and have shallower bank heights in this part of the delta, leading to increased cross-Delta and along-channel hydraulic gradients; and/or (ii) a proportion of the Peel River flow is lost to the Middle Channel due to lateral drainage across the Delta through distributary channels. Whatever the cause, this is a valuable observation because there are no hydrometric stations in this part of the Delta, and the channel hydraulics here are not well understood. This illustrates the potential of one-time LiDAR WL mapping as a means to support hydrometric station site selection.

The LiDAR WL data have facilitated interesting observations on the flow hydraulics at the local scale (Peel at Aklavik) and Delta scale (South Transect WLs) that are not represented in field or hydrometric records, and would be challenging to acquire by other means. It should be noted, however, that the implications of this study go beyond the Mackenzie Delta. Archives of airborne LiDAR data covering large areas of terrain, lakes, river channels, and wetlands exist for entire countries, states, and provinces in Europe and North America (e.g. Airborne Imaging, 2010). The size and accessibility of these databases are growing continually. While this study has focussed on in-channel water levels, it is clear that lake and wetland water surface elevations can also be mapped over similarly small extents and at high resolution. Therefore, if archive LiDAR data exist over complex wetland systems where regional gradients or hydrological connectivity are not well understood, then it is suggested that researchers take another look at these datasets to see what additional hydrological and hydraulic information can be obtained by mapping the water surfaces and not just the surrounding terrain, as is typically the case.

## ACKNOWLEDGEMENTS

We thank Allyson Fox (AGRG) for LiDAR operations and data support; JC Lavergne (Geodetic Survey Division, NRCan) and James Churchill (AGRG) for field support; Mark Russell (NHRI, Environment Canada) and George Lennie (Water Survey of Canada, Environment Canada) for hydrometric data; Mike Craymer (Geodetic Survey Division, NRCan) for GPS data processing; and Gavin Manson and Dustin Whalen (Geological Survey of Canada, NRCan) for helpful reviews. LiDAR hardware was funded through the Canada Foundation for Innovation. Funding was provided to Lesack through IPY-SCARF and to Forbes through ArcticNet and the NCE program. The LiDAR acquisition and processing were funded jointly by EC, NRCan, and INAC. Some local logistical support was provided by the Aurora Research Institute. This is ESS contribution No. 20100453 [Crown copyright reserve].

## REFERENCES

Airborne Imaging, 2010. *Airborne Imaging LiDAR coverage of Western Canada.* http://www.airborneimaginginc.com/data_coverage_alberta.htm Last accessed: 20 April 2011.

Alsdorf DE, Bates P, Melack J, Wilson M, Dunne T. 2007a. Spatial and temporal complexity of the Amazon flood measured from space. *Geophysical R esearch Letters* **34**: L08402, DOI:10.1029/2007GL029447.

Alsdorf DE, Rodriguez E, Lettenmeier DP. 2007b. Measuring surface water from space. *Reviews of Geophysics* **45**: 1–24.

 

Andersen HE, Reutebuch SE, McGaughey RJ. 2006. A rigorous assessment of tree height measurements obtained using airborne lidar and conventional field methods. *Canadian Journal of Remote Sensing* **32**(5): 355–366.

Applanix Inc. 2008. *POSMMS software manual*. Applanix Incorporated: Toronto; 514.

Axelsson P. 2000. DEM generation from laser scanner data using adaptive TIN models, *International Archives of Photogrammetry and Remote Sensing*, **XXXIII**: B4: 110–117.

Baghdadi N, Lemarquand N, Abdallah H, Bailly JS. 2011. The Relevance of GLAS/ICESat Elevation Data for the Monitoring of River Networks. *Remote Sensing* **3**: 708–720.

Birkett CM. 2000. Synergistic remote sensing of Lake Chad: Variability of basin inundation. *Remote Sensing of Environment* **72**: 218–236.

Birkett CM, Mertes LAK, Dunne T, Costa MH, Jasinski MJ. 2002. Surface water dynamics in the Amazon Basin: application of satellite radar altimetry. *Journal of Geophysical Research* **107**(D20): 8059, DOI:10.1029/2001JD000609.

Bowen ZH, Waltermire RG. 2002. Evaluation of light detection and ranging (LIDAR) for measuring river corridor topography. *Journal of the American Water Resources Association* **38**: 33–41.

Brennen R, Webster T. 2006. Object-oriented land cover classification of lidar-derived surfaces. *Canadian Journal of Remote Sensing* **32**(2): 162–172.

Brzank A, Heipke C. 2006. Classification of Lidar Data into water and land points in coastal areas. *International Archives of Photogrammetry and Remote Sensing* **36**(3): 197–202.

Burman H. 2002. Laser strip adjustment for data calibration and verification, *International Archives of Photogrammetry and Remote Sensing* **34**(3): A-67–72.

Carter WE, Shrestha RL, Tuell G, Bloomquist D, Sartori M. 2001. Mapping the surface of sheet flow in the Everglades. *International Archives of Photogrammetry and Remote Sensing* **34**(3): 175–180.

Cohen SJ. 1997. What if and so what in northwest Canada: could climate change make a difference to the future of the Mackenzie Basin? *Arctic* **50**(4): 293–307.

Crasto N. 2011. *Hydrological feature delineation and water level estimation in the Mackenzie Delta, NWT using digital terrain analyses on airborne lidar derived data*. Unpublished M.Sc. thesis. Acadia University; p. 167.

Durand M, Fu LL, Lettenmaier DP, Alsdorf D, Rodríguez E, Esteban-Fernandez D. 2010. The surface water and ocean topography mission: observing terrestrial surface water and oceanic submesoscale eddies. *Proceedings of the IEEE* **98**(5): 766–779.

Emmerton CA, Lesack LFW, Marsh P. 2007. Lake abundance, potential water storage and habitat distribution in the Mackenzie River Delta, western Canadian arctic, *Water Resources Research* **43**(W05419): 1–14.

Forbes DL, Craymer MR, James TS, Solomon SM, Marsh P, Manson GK, Whalen D, Hopkinson C. 2010. Sea-level rise, subsidence and potential inundation on the outer Mackenzie Delta. *Proceedings IPY Oslo Science Conference, Polar Science—Global Impact*, Oslo, 8–12 June 2010 (abstract on-line at http://ipy-osc.no/abstract/383055, accessed 2011-01-21).

French JR. 2003. Airborne lidar in support of geomorphological and hydraulic modelling. *Earth Surface Processes and Landforms* **28**: 321–335.

Furgal C, Prowse TD. 2008. Northern Canada. In *From Impacts to Adaptation: Canada in a Changing Climate 2007*, Lemmen DS, Warren FJ, Lacroix J, Bush E (eds). Government of Canada: Ottawa; pp. 57–118.

Galand P, Lovejoy C, Vincent, WF. 2006. Remarkably diverse and contrasting archaeological communities in a large arctic river and the coastal Arctic Ocean. *Aquatic Microbial Ecology* **44**: 115–126.

Genc L, Smith SE, Dewitt BA. 2005. Using satellite imagery and lidar data to corroborate an adjudicated ordinary high water line. *International Journal of Remote Sensing* **26**(17): 3683–3693.

Goulden T, Hopkinson C. 2010. The forward propagation of integrated system components within airborne lidar data. *Photogrammetric Engineering and Remote Sensing* **76**(5): 598–601.

Goulding H, Prowse T, Beltaos S. 2009. Spatial and temporal patterns of break-up and ice-jam flooding in the Mackenzie Delta, NWT. *Hydrological Processes* **23**: 2654–2670. DOI:10.1002/hyp.7251.

Guenther GC, Brooks MW, LaRocque PE. 2000. New capabilities of the 'SHOALS' airborne lidar bathymeter. *Remote Sensing of Environment* **73**(2): 247–255.

Hicks F, Chen X, Andres D. 1995. Effects of ice on hydraulics of Mackenzie River at the outlet of Great Slave Lake, N.W.T.: a case study. *Canadian Journal of Civil Engineering* **22**: 43–54.

Hill PR, Lewis CP, Desmarais S, Kauppaymuthoo V, Rais H. 2001. The Mackenzie delta: Sedimentary processes and facies of a high-latitude, fine-grained delta. *Sedimentology* **48**: 1047–1078.

Hofle B, Vetter M, Pfeifer N, Mandlburger G, Stotter J. 2009. Water surface mapping from airborne laser scanning using signal intensity and elevation data. *Earth Surface Processes and Landforms* **34**: 1635–1649.

Hollaus M, Wagner W, Kraus K. 2005. Airborne laser scanning and usefulness for hydrological models. *Advances in Geosciences* **5**: 57–63.

Hopkinson C. 2007. The influence of flying altitude and beam divergence on canopy penetration and laser pulse return distribution characteristics. *Canadian Journal of Remote Sensing* **33**(4): 312–324.

Hopkinson C, Chasmer LE, Zsigovics G, Creed I, Sitar M, Kalbfleisch W, Treitz P. 2005. Vegetation class dependent errors in LiDAR ground elevation and canopy height estimates in a Boreal wetland environment. *Canadian Journal of Remote Sensing* **31**(2): 191–206.

Hwang P, Krabill W, Wright W, Swift R, Walsh E. 2000. Airborne scanning lidar measurement of ocean waves. *Remote Sensing of Environment* **73**: 236–246.

Ivanov V. 1970. Hydraulic calculation of water discharge and levels in river deltas. *IAHS Red Book No. **91**: Hydrology of Deltas. Proceedings of the Bucharest Symposium*, 6–14 May 1969; 239–245.

Lane SN, Bradbrook KF, Richards KS, Biron PM, Roy AG. 2000. Secondary circulation cells in river channel confluences: measurement artefacts or coherent flow structures. *Hydrological Processes* **14**: 2047–2071.

Lesack L, Marsh P. 2010. River-to-lake connectivities, water renewal, and aquatic habitat diversity in the Mackenzie River Delta. *Water Resources Research* **46**: W12504, DOI:10.1029/2010WR009607; 16.

Lesack LFW, Marsh P. 2007. Lengthening plus shortening of river-to-lake connection times in the Mackenzie River Delta respectively via two global change mechanisms along the arctic coast. *Geophysical Research Letters* **34**: L23404, DOI:10.1029/2007GL031656.

Lesack L, Marsh P, Hicks F, Beltaos S, Forbes D, Gareis J, Hopkinson C, Nafziger J, Perrie W, Roberts A, Solomon S, van der Sanden J, Carter T, Haywood H, Russell M, Pilling R, Ross D. 2010. Study of Canadian Arctic river-delta fluxes (IPY-SCARF): resolving Mackenzie River nutrient fluxes to the Arctic Ocean. *Proceedings IPY Oslo Science Conference, Polar Science—Global Impact*, Oslo, 8–12 June 2010 (abstract on-line at http://ipy-osc.no/abstract/383386, accessed 2011-01-21).

Mackay JR. 1963. *The Mackenzie Delta area, N.W.T*. Misc. Report 23, Geological Survey of Canada: Ottawa; p. 202.

Magirl CS, Webb RH, Griffiths PG. 2005. Changes in the water surface profile of the Colorado River in Grand Canyon, Arizona, between 1923 and 2000. *Water Resources Research* **41**: DOI:10.1029/2003WR002519.

Mandlburger G, Briese C. 2007. Using airborne laser scanning for improved hydraulic models. In *International Congress on Modeling and Simulation*, Christchurch, New Zealand, vol. MODSIM07.

Marks K, Bates P. 2000. Integration of high-resolution topographic data with floodplain flow models. *Hydrological Processes* **14**: 2109–2122.

Marsh P, Hey M. 1989. The flooding hydrology of Mackenzie Delta lakes. *Arctic* **42**(1): 41–49.

Marsh P, Lesack L, Hicks F, Roberts A, Hopkinson C, Solomon S, Forbes D, Russell M, Haywood H. 2010. Hydrology of the Mackenzie Delta: off-channel water storage and delta interaction with the Beaufort Sea. *Proceedings of the 17th International Northern Research Basins Symposium and Workshop, 2009*; pp. 217–226.

Martin CF, Thomas RH, Krabill WB, Manizade SS. 2005. ICESat range and mounting bias estimation over precisely-surveyed terrain. *Geophysical Research Letters* **32**: L21S07.

McCullagh MJ. 1981. Creation of smooth contours over irregularly distributed data using local surface patches, *Geophysical Analysis* **13**: 51–63.

Morris CS, Gil SK. 1994. Evaluation of the TOPEX/Poseidon altimeter system over the Great lakes. *Journal of Geophysical Research* **99**: 24527–24539.

MRBC. 1981. Mackenzie River basin. In *Mackenzie River Basin Study Report*. Mackenzie River Basin Committee: Ottawa; pp. 7–67.

Nafziger J, Hicks F, Andrishak R, Marsh P, Lesack L. 2010. Hydraulic model of river flow and storage effects in the Mackenzie Delta, Canada. *Proceedings of the 17th International Northern Research Basins Symposium and Workshop, 2009*; pp. 237–247.

Optech Inc. 2004. *ALTM 3100 Specifications*. Optech Incorporated: Toronto; 4.

 

Pavelsky TM, Smith LC. 2008. Remote sensing of hydrologic recharge in the Peace-Athabasca Delta, Canada. *Geophysical Research Letters* **35**: L08403, DOI:10.1029/2008GL033268.

Petrie G, Toth CK. 2009. Terrestrial laser scanners. In *Topographic Laser Ranging and Scanning—Principles and Processing*, Shan J, Toth K (eds). CRC Press, Taylor & Francis Group: Boca Raton; p. 590.

Shepard D. 1968. A two-dimensional interpolation function for irregularly-spaced data. *Proceedings of the 1968 Association for Computing Machinery National Conference*; 517–524.

Shrestha RL, Carter WE, Lee M, Finer P, Sartori M. 1999. Airborne laser swath mapping: Accuracy assessment for surveying and mapping applications. *Journal of the American Congress on Surveying and Mapping* **59**(2): 83–94.

Smith LC. 1997. Satellite remote sensing of river inundation area, stage, and discharge: a review. *Hydrological Processes* **11**: 1427–1439.

Spence C, Sasco P. 2005. A hydrological neighbourhood approach to predicting streamflow in the Mackenzie Valley. In *Prediction in ungauged basins: approaches for Canada's cold regions*, Spence C, Pomeroy J, Pietroniro A, Shook K, Marks D (eds). Canadian Water Resources Association: Saskatoon, Canada; pp. 21–44.

Squires M, Lesack L, Hecky R, Guildford S, Ramlal P, Higgins S. 2009. Primary production and carbon dioxide metabolic balance of a lake-rich arctic river floodplain: partitioning of phytoplankton, epipelon, macrophyte, and epiphyton production among lakes of the Mackenzie Delta. *Ecosystems* **12**: 853–872. DOI:10.1007/s10021-009-9263-3.

Töyrä J, Pietroniro A, Hopkinson C, Kalbfleisch W. 2003. Assessment of airborne scanning laser altimetry (lidar) in a deltaic wetland environment. *Canadian Journal of Remote Sensing* **29**(6): 718–728.

Urban TJ, Schutz BE, Neuenschwander AL. 2008. A survey of ICESat coastal altimetry applications: Continental coast, open ocean island, and inland river. *Terrestrial Atmospheric Oceanic Sciences* **19**: 1–19.

Véronneau M, Mainville A, Craymer MR. 2002. *The GPS Height Transformation (v2.0): An Ellipsoidal- CGVD28 Height Transformation for Use with GPS in Canada*. Geodetic Survey Division, Earth Sciences Sector, Natural Resources Canada: Ottawa.

Véronneau M, Duval R, Huang J. 2006. A gravimetric geoid model as a vertical datum in Canada. *Geomatica* **60**(2): 165–172.

Vosselman G. 2000. Slope based filtering of laser altimetry data. *International Archives of Photogrammetry and Remote Sensing*, Vol. **XXXIII**: B3: 935–942.

Wagner W, Ullrich A, Melzer T, Briese C, Kraus K. 2004. From single-pulse to full-waveform airborne laser scanners: Potential and practical challenges. *Archives of Photogrammetry and Remote Sensing* **35**(B/3): 201–206.

Wehr A, Lohr U. 1999. Airborne laser scanning—an introduction and overview. *ISPRS Journal of Photogrammetry and Remote Sensing* **54**: 68–82.

World Meteorological Organisation, 2010. *Manual on stream gauging. Volume 1—Fieldwork. WMO-No. 1044*, World Meterological Organization: Geneva, Switzerland; pp. 248.

 

## APPENDIX 1. LIDAR PROCESSING AND ELEVATION CONTROL

Multiple GPS base stations were set up around the polygons to provide ground control for the airborne survey. All GPS base station coordinates were processed relative to the first order active control stations at Inuvik, Tuktoyuktuk and Yellowknife by the Geodetic Survey Division (GSD) of Natural Resources Canada. The first data processing task was to differentially correct the aircraft GPS trajectories relative to the ground network of base stations. Raw laser pulse return ranges and scan angles were integrated with aircraft trajectory and sensor orientation data using *PosMMS* (Applanix, 2008) and *Dashmap* (Optech, 2004) proprietary software tools. The outputs from these procedures were a series of flight line data files containing t, x, y, z, i (universal time, easting, northing, elevation, intensity) information for each laser pulse return collected from the ground or canopy environment being sampled.

All data were projected into UTM coordinates (zone 8) relative to the NAD83 horizontal datum, with elevations initially defined relative to the ellipsoid (GRS80) as this was the native datum of the GPS positioning network. The point cloud data were then imported into the *Terrascan* (Terrasolid, Finland) software package for data cleaning, tiling, strip matching (Burman, 2002), and ground classification using a morphological ground classification filter (Axelsson, 2000; Vosselman, 2000) to provide a digital elevation model (DEM). Given the hydrological nature of the study, elevations were converted from ellipsoidal heights (h) to orthometric heights (H) relative to the CGVD28 datum using the HTv2·0 transformation tool developed by GSD. The tool is based on the CGG (Canadian Gravimetric Geoid) 2000 model plus a correction surface (HRG01) to force the transformed elevations to align with published CGVD28 benchmark elevations (Véronneau *et al*., 2002). The actual transformation performed was:

$$H = h - N \tag{A1}$$

where $N$ = geoid height or undulation. The updated and hydrologically more accurate CGG05 model (Véronneau *et al*., 2006) was not available to the authors at the time of initial LiDAR data processing. However, water level data were made available to this study in orthometric heights computed using the CGG05 model (Mark Russell, Environment Canada, pers. comm. 2010). Owing to model availability at time of LiDAR processing, a further minor transformation of the CGVD28 LiDAR water level data was necessary to account for the slight (mm to cm range) difference in the equipotential surface definition between the CGG05 and HTv2·0 (CGG00 + HRG01) models (Véronneau *et al*., 2006).

$$\mathrm{H}_{(\mathrm{CGG05})} = \mathrm{H}_{(\mathrm{HTv2{\cdot}0})} + \mathrm{N}_{(\mathrm{HTv2{\cdot}0})} - \mathrm{N}_{(\mathrm{CGG05})} \tag{A2}$$

The HTv2·0 transformation model is known to contain small inaccuracies and a more up-to-date transformation using the CGG05 model is reported to provide hydrologically more accurate results (Verroneau *et al*., 2006). It was important, therefore, to quantify the bias introduced by using HTv2·0 and evaluate whether this bias could have any discernible impact on the WL gradients estimated from LiDAR. The elevation differences between the two equipotential surfaces are provided for the east and west extremities of each survey area in Table AI.

In all cases, the vertical bias introduced by adopting the HTv2·0 never exceeds 0·12 m, and the maximum deviation between the two orthometric transformation models is found to be 0·15 m across the full 70 km width of the Inuvik Transect. This is the largest gradient to be seen both within any of the polygons and between the polygons. The gradient associated with this maximum deviation is $2{\cdot}0 \times 10^{-6}$ m m$^{-1}$. This is approximately an order of magnitude lower than the longitudinal gradients in this part of the Delta and is within the range of noise for lateral gradients. The elevation and gradient bias for all other areas is smaller, and indeed for the Outer Delta where the lowest actual hydraulic gradients are experienced, the difference between the two equipotential surfaces has no discernible slope in any direction. Consequently, the error introduced by applying the HTv2·0 transformation will not have introduced any appreciable error into WL gradients across or along the Delta. Nonetheless, the 0·15 m range experienced in the centre of the Delta is larger than the observed noise level and bias in the LiDAR data, so it is recommended that any future hydraulic analyses using these datasets should apply the CGG05 transformation.

## APPENDIX 2. LIDAR TERRAIN SURFACE VALIDATION

To place the presented water level validation into context, it was necessary to establish how accurate the LiDAR data were over typical terrain surfaces in the Mackenize Delta region. A control surface was set up over the airport runway at Inuvik and ten ground surface validation profiles were surveyed within the Inuvik transect and the Taglu survey polygons. An attempt was made to represent the diversity of ground covers in the Delta, but placement was limited to areas that had LiDAR data coverage and were accessible by road, motorboat or helicopter. In areas where the sky view was unobstructed, post-processed kinematic (PPK) GPS survey points were collected at 5 m increments along a 60 m tape measure.

Table AI. Differences in equipotential height between HTv2·0 (CGG00 + HRG01) and CGG05 at key locations within the Mackenzie Delta

| | South Transect | Inuvik Transect | North Transect | Outer Delta polygon |
|---|---|---|---|---|
| West | 0·04 | 0·003 | −0·01 | −0·04 |
| East | −0·06 | −0·12 | −0·06 | −0·04 |
| Range | 0·10 | 0·15 | 0·05 | 0·00 |

At each measurement interval, the vegetation cover (if any) and height were recorded, and ground surface condition visibly noted as either dry or saturated. In spruce and mixed wood canopy-covered areas, profiles were established over flat ground with rapid static GPS measurements made at either end. For the canopy-covered profiles, vegetation type (hardwood, softwood or mixed) and height (using a Vertex hypsometer) were recorded at 5 m increments.

From the four flights where it was possible to overfly the Inuvik Airport runway ground control surface either before or after a survey mission, a mean bias of −0·05 m and RMSE of 0·08 m was recorded (Table AII). The bias was strongly influenced by the data collected on the first day, with two of the days having LiDAR and ground control surfaces within 0·02 m. These results are well within the manufacturer quoted system accuracy specification of 0·15 m for the approximate 1000 m altitude of overflight (Optech, 2004), and were also well within expected one-sigma-system noise levels (Goulden and Hopkinson, 2010). Moreover, any data collected close to the start or end of a flight may have had reduced forward and reverse GPS initialisation time and so have the potential to be degraded (Applanix, 2008). Consequently, there was *a priori* no justification to apply an elevation correction to the LiDAR data, as they already represented terrain elevations over flat unvegetated control surfaces at the expected level of accuracy.

The runway validation results in Table AII represent an optimal control surface which is flat, solid and has no vegetation cover to interfere with a laser pulse return signal. The terrain surface validation over more natural surfaces experienced within the Delta is presented in Table AIII. LiDAR elevation bias ranges from −0·09 m over a saturated marsh surface to +0·28 m for a spruce canopy and dense shrub covered surface. In general, those areas with either a vegetative over-storey or ground-level under-storey display the greatest errors and a significant positive elevation bias. The pattern and magnitude of these results are consistent with previous observations over forested (Anderson *et al*., 2006), river corridor (Bowen and Waltermire, 2002), boreal wetland (Hopkinson *et al*., 2005) and northern delta (Töyrä *et al*., 2003) environments. Marsh, open gravel pad and short grass, and herbaceous surfaces demonstrate the least bias and this is likely because there is minimal vegetation height and horizontally projected foliage to interfere with the incident laser pulse. The negative elevation biases at the marsh and mixed wood sites are noteworthy and could suggest that the negative bias observed in the runway validation data (Table AII) exists within data collected over the Delta as well. However, the mixed wood sampling transect that displays a −0·09 m bias was surveyed with static GPS beneath canopy cover at two end points with the ground in between assumed to be flat. GPS error is expected to be amplified beneath canopy due to multipath and reduced satellite visibility, and it is possible that some small decimetre-level error crept into the ground validation on this profile. Given the relative high standard deviation of 0·2 m, this negative bias cannot be taken as absolute. The −0·05 m bias at the Inuvik marsh site was not repeated at the Outer Delta marsh site. Furthermore, of the ground validation profiles sampled, the gravel pad was the only one that was completely flat and devoid of any vegetation cover and here the LiDAR and field data agree to within 0·01 m with no significant difference at the 95% level of confidence. Consequently, the observed slight underestimates of elevation provide no justification for a systematic correction of the entire LiDAR dataset.

Table AII. Ground validation statistics for each day of survey flights collected at the Inuvik Airport runway. No elevation corrections could be justified based on these results

| | Inuvik runway validation | | | | |
|---|---|---|---|---|---|
| | 11 Aug | 13 Aug | 15 Aug | 16 Aug | Combined |
| **Average $\delta z$ (m)** | −0·11 | −0·05 | −0·01 | −0·02 | −0·05 |
| **$\sigma$ (m)** | 0·05 | 0·03 | 0·09 | 0·04 | 0·05 |
| **n** | 2047 | 2047 | 2047 | 2047 | 8188 |
| **RMSE (m)** | **0·12** | **0·05** | **0·09** | **0·04** | **0·08** |

Table AIII. Landcover stratified terrain elevation validation results collected along sampling profiles over the Inuvik Transect and Outer Delta polygons

| | Inuvik polygon | | | | | Outer Delta polygon | | | |
|---|---|---|---|---|---|---|---|---|---|
| | Ivk 1 spruce/shrub | Ivk 2 spruce/shrub | Ivk 3 mixed wood | Ivk 4 mixed wood | Ivk 5 marsh | OD 1 gravel | OD 2 marsh | OD 3 willow/shrub | OD 4 grass/herbs |
| **Average $\delta z$ (m)** | 0·14 | 0·28 | −0·09 | 0·11 | −0·05 | −0·01 | 0·01 | 0·18 | 0·10 |
| **$\sigma$ (m)** | 0·12 | 0·17 | 0·20 | 0·13 | 0·15 | 0·03 | 0·05 | 0·13 | 0·05 |
| **n** | 13 | 13 | 9 | 4 | 13 | 13 | 13 | 13 | 12 |
| **RMSE (m)** | **0·18** | **0·32** | **0·21** | **0·17** | **0·19** | **0·03** | **0·04** | **0·22** | **0·11** |